blood®
Regular Article

LYMPHOID NEOPLASIA

Nanoromidepsin, a polymer nanoparticle of the HDAC inhibitor, improves safety and efficacy in models of T-cell lymphoma

Ipsita Pal,[1-3] Anuradha Illendula,[1-3] Andrea Joyner,[1-3] John Sanil Manavalan,[1,2] Tess M. Deddens,[1-3] Ariana Sabzevari,[1-3] Deepthi P. Damera,[1-3] Samir Zuberi,[1-3] Enrica Marchi,[1-3] Todd E. Fox,[2,4] Marya E. Dunlap-Brown,[5] Kallesh D. Jayappa,[1-3] Jihane Khalife,[1-3] Jeffrey W. Craig,[6] Thomas P. Loughran Jr,[1-3] David J. Feith,[1-3] and Owen A. O'Connor[1-3,7]

[1]University of Virginia Comprehensive Cancer Center, [2]Division of Hematology and Oncology, [3]Translational Orphan Blood Cancer Research Center, [4]Department of Pharmacology, [5]Molecular Immunologic and Translational Sciences Core, [6]Department of Pathology, and [7]Department of Microbiology, Immunology and Cancer Biology, University of Virginia, Charlottesville, VA

KEY POINTS

- **The treatment options for patients with relapsed or refractory PTCL are dwindling, given the paucity of drugs available for these patients.**
- **Leveraging a novel polymer nanochemistry platform, we synthesized a new epigenetic modulator with superior features in T-cell malignancies.**

Histone deacetylase inhibitors (HDACis) are valued treatment options for patients with T-cell malignancies. Romidepsin is a selective class I HDACi initially approved for patients with relapsed or refractory cutaneous and peripheral T-cell lymphomas (PTCLs). Romidepsin was withdrawn from its PTCL indication following a negative randomized phase 4 study (romidepsin-CHOP [cyclophosphamide, doxorubicin hydrochloride (hydroxydaunorubicin), vincristine sulfate (Oncovin), and prednisone]) that showed no benefit over CHOP alone, further diminishing options for patients. Herein, we describe the development of, to our knowledge, a first-in-class polymer nanoparticle (PNP) of romidepsin using an innovative amphiphilic diblock copolymer–based nanochemistry platform. Nanoromidepsin exhibited superior pharmacologic properties with improved tolerability and safety in murine models of T-cell lymphoma (TCL). The PNP also exhibited superior antitumor efficacy in multiple models, including in vitro TCL cell lines, ex vivo samples from patients with large granular lymphocyte (LGL) leukemia, and murine TCL xenografts. Nanoromidepsin demonstrated greater accumulation in tumors and a statistically significant improvement in overall survival compared with romidepsin in murine xenograft models. These findings justify the clinical development of nanoromidepsin in patients with T-cell malignancies.

Introduction

The histone deacetylase inhibitors (HDACis) are important drugs for the treatment of T-cell lymphoma (TCL). Four HDACis have been approved globally for patients with relapsed/refractory (R/R) cutaneous and peripheral T-cell lymphomas (PTCLs). Although HDACis induce cytotoxicity across many types of malignant disease, clinically their benefits have been confined to patients with TCL. HDACs catalyze the deacetylation of histone and nonhistone proteins. Deacetylation of histone leads to the condensation of chromatin (heterochromatin) and transcriptional repression.[1] HDACis prevent deacetylation of histones such as histone-3 (H3) and H4, promoting open chromatin (euchromatin) and transcriptional activation.

There are 11 isoforms of HDAC, classified as I, IIA, IIB, III, and IV. Class III HDACs are not affected by any of the available HDACis and are referred to as sirtuins, which are known to deacetylate p53. Romidepsin exhibits nanomolar potency against class I HDACs, whereas most other HDACi would be considered pan-HDACis.[2] Although the dissociation constant (K_d) of any HDACis against a particular isoform may vary, it is clear that the profiles of genes activated or repressed by the different HDACis can vary significantly as a function of the HDACi, its concentration, its duration of exposure, and the disease-specific context. Efforts to ascribe inhibition of a particular HDAC isoform to clinical outcomes have been largely unsuccessful. As a result, these drugs are often considered pleiotropic as they induce a broad spectrum of cellular effects. Complicating this pharmacology is the recognition that HDACs can also deacetylate a host of nonhistone proteins such as B-cell lymphoma 6 (Bcl-6).[3] The implications of these effects in any given disease are presently unclear.

Despite the reproducible activity of these drugs in patients with R/R PTCL, a recent phase 3 trial of romidepsin-CHOP (cyclophosphamide, doxorubicin hydrochloride [hydroxydaunorubicin], vincristine sulfate [Oncovin], and

prednisone) vs CHOP reported no difference in progression-free survival (PFS) or overall survival (OS) between the arms, resulting in withdrawal of the PTCL indication.[4] This, coupled with the recognition that other drugs for R/R PTCLs are in regulatory jeopardy, has created legitimate concerns over future management options.

Nanoparticle-based drug design offers the prospect of improved pharmacologic properties, tumor penetration, and intertumoral drug retention with reduced degradation and toxicities.[5] In particular, the development of amphiphilic block copolymer nanoparticles (PNPs) has expanded the repertoire of drugs that can leverage the advantages of nanotherapeutics.[6] We sought to overcome historic liabilities associated with romidepsin, while capitalizing on the benefits of a novel nanochemistry platform. To our knowledge, we report the development of the first PNP of romidepsin and demonstrate the superior safety, targeted delivery, and efficacy of the PNP.

Materials and methods

Fabrication of nanoromidepsin

We adopted a tandem parallel synthesis to achieve optimal nanoromidepsin physicochemical properties (>500 μg/mL romidepsin, <100 nm particle size, and <0.2 polydispersity index [PDI]) using a versatile nanoprecipitation method. We explored the influence of selected parameters of the nanoprecipitation method, including solvent-to-antisolvent ratio and drug-to-polymer ratio, to produce romidepsin-loaded nanoparticles meeting the predetermined criteria. For biodistribution studies, we coloaded nanoromidepsin and the fluorescent tracer 3,3′-Dioctadecyloxacarbocyanine perchlorate (DiO) into PNPs as previously described (see supplemental Materials and methods, available on the *Blood* website, for details).

Single- and multiple-dose in vivo toxicity study

For single-dose maximum tolerated dose (MTD) studies, BALB/c mice (n = 5) received nanoromidepsin or romidepsin via a single intraperitoneal (IP) or IV dose (1-10 mg/kg), with 14-day monitoring. For repeat-dose studies, NOD.Cg-*Prkdc*^{scid} *Il2rg*^{tm1Wjl}/SzJ (NSG) mice engrafted with a TCL cell line expressing dTomato and luciferase (H9-dTomato-Luc) cells were treated with ghost PNP, romidepsin, or nanoromidepsin using various IV dosing regimens (supplemental Methods). Toxicity was assessed by tracking weight loss and clinical scores over time.

Pharmacokinetic (PK) study

Five- to seven-week-old female BALB/c mice were treated with IV or IP nanoromidepsin or romidepsin. Animals (n = 21) received a single dose of one-half MTD as defined by the single-dose toxicity study (2.5 mg/kg body weight) of nanoromidepsin or romidepsin. Mice were euthanized (n = 3 per time point) at 1, 3, 6, 18, 24, 48, and 72 hours after the treatment. Collection of plasma and quantification of romidepsin is described in the supplemental Methods.

Biodistribution study

Biodistribution of nanoromidepsin was evaluated in H9-dTomato-Luc xenograft. Tumor-bearing NSG mice were randomly assigned into 2 groups (n = 3) and injected IV with nanoromidepsin coloaded with DiO or free DiO at an equivalent dose (3.7 mg/kg). Whole-body fluorescence imaging was performed on a cryogenically cooled Lago X (Spectral Instruments Imaging system). Three mice from each group were killed after 72 hours. Tumors and vital organs were harvested for ex vivo imaging.

Survival and efficacy study

H9-dTomato-Luc engrafted mice were randomized to 4 treatment groups of 9 mice each: (1) phosphate buffered saline (PBS) control, (2) ghost PNP, (3) romidepsin (3.5 mg/kg), or (4) nanoromidepsin (3.5 mg/kg) after the minimum tumor luminescence reached 10^6 bioluminescence imaging intensity (BLI; photons per second per square centimeter per steradian). All drugs were administered by tail vein once a week. Baseline BLI was completed for all mice the day before the first treatment. In vivo BLI analysis was conducted on Lago X (Spectral Instruments Imaging system). A second efficacy/survival study was performed using similar methods with groups with 4 mg/kg (n = 9).

Statistical analysis

Results are presented as the mean ± standard deviation, unless indicated otherwise. Statistical significance was determined by 1-way analysis of variance or 2-tailed Student *t* test or log-rank test, unless specified otherwise, using GraphPad Prism software, and a *P* value of <.05 was considered statistically significant.

Results

Engineering of nanoromidepsin-loaded PNP

Different PNPs of romidepsin were synthesized using generally regarded as safe amphiphilic diblock copolymers or US Food and Drug Administration–approved lipids for liposomes. Liposomes did not achieve romidepsin encapsulation and were not pursued further. PNPs were synthesized using methoxy poly (ethylene glycol)-b-poly (D, L-lactide) (mPEG-PDLLA) and methoxy poly (ethylene glycol)-b-poly (lactide-co-glycolide) (mPEG-PLGA), and the surfactant poloxamer-188 using a solvent displacement or nanoprecipitation technique. Liquid chromatography-mass spectrometry (LC-MS) confirmed an average romidepsin concentration in optimized PNPs of >500 μg/mL (Figure 1A). mPEG-PDLLA nanoparticles exhibited higher drug concentrations (~540 μg/mL) with an average drug encapsulation efficiency of 48%. Cryo-electron microscopy (cryo-EM) revealed that both ghost and romidepsin-loaded PNPs exhibited uniform spherical morphology and homogeneous size with no agglomeration (Figure 1B). Dynamic light scattering revealed a unimodal distribution of particles with an average size of 46.25 nm and a PDI of 0.145 (Figure 1C-D).

The concentration-response relationship for each PNP was compared with romidepsin across a panel of TCL lines and a reference solid tumor cell line (Figure 1E). All 3 PNPs of romidepsin reduced cell viability in a concentration-dependent manner (Figure 1E), though the 50% inhibitory concentration (IC_{50}) values for different PNPs varied across lines (Figure 1F). At 60 hours, most cell lines were consistently sensitive to nanoromidepsin mPEG-PDLLA H_2O (IC_{50} = 0.7-1.9 nM), which

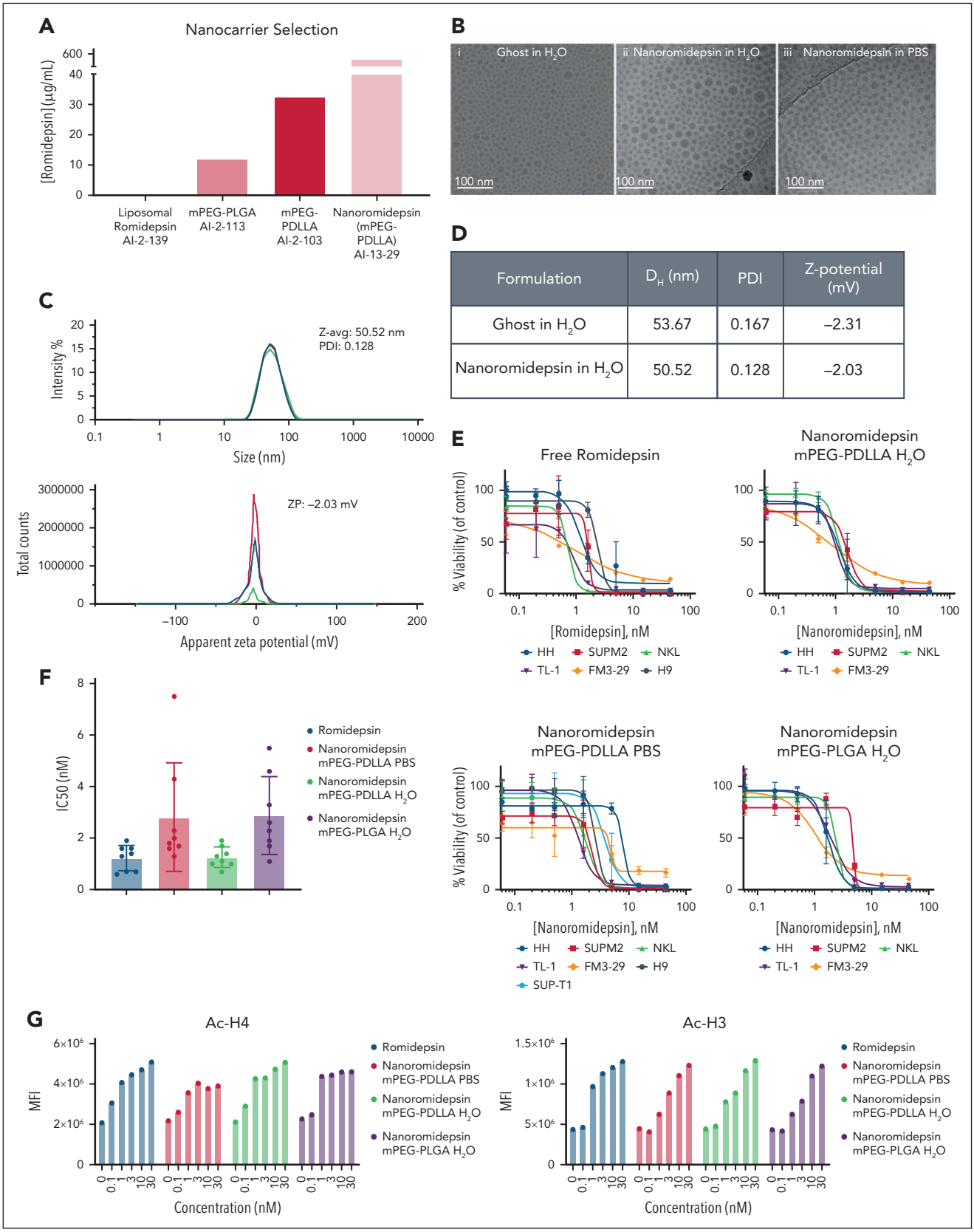

Figure 1. Romidepsin nanoparticle synthesis, physicochemical characterization, and drug activity analysis in PTCL cells in vitro. (A) Carrier selection screening. Romidepsin encapsulation quantified by LC-MS. (B) Cryo-EM of different analogs of nanoromidepsin to identify the size and morphology of PNPs synthesized in different solvents; (i) Ghost in H_2O, (ii) nanoromidepsin in H_2O, (iii) nanoromidepsin in PBS. (C) Dynamic light scattering (DLS) graphs (top) and ZP (bottom) spectra of nanoromidepsin in H_2O. (D) DLS and ZP data of nanoromidepsin ghost and nanoromidepsin in H_2O. (E) HH and H9 (cutaneous TCL [CTCL]), SUPM2 (anaplastic lymphoma kinase positive anaplastic large cell lymphoma [ALK^+ ALCL]) TL-1 (LGL leukemia), NKL, FM3-29 (melanoma) were treated with romidepsin and different analogs of nanoromidepsin (mPEG-PDLLA nanoromidepsin H_2O, mPEG-PDLLA nanoromidepsin PBS, and mPEG-PLGA nanoromidepsin H_2O) to explore the impact on the cell viability of different

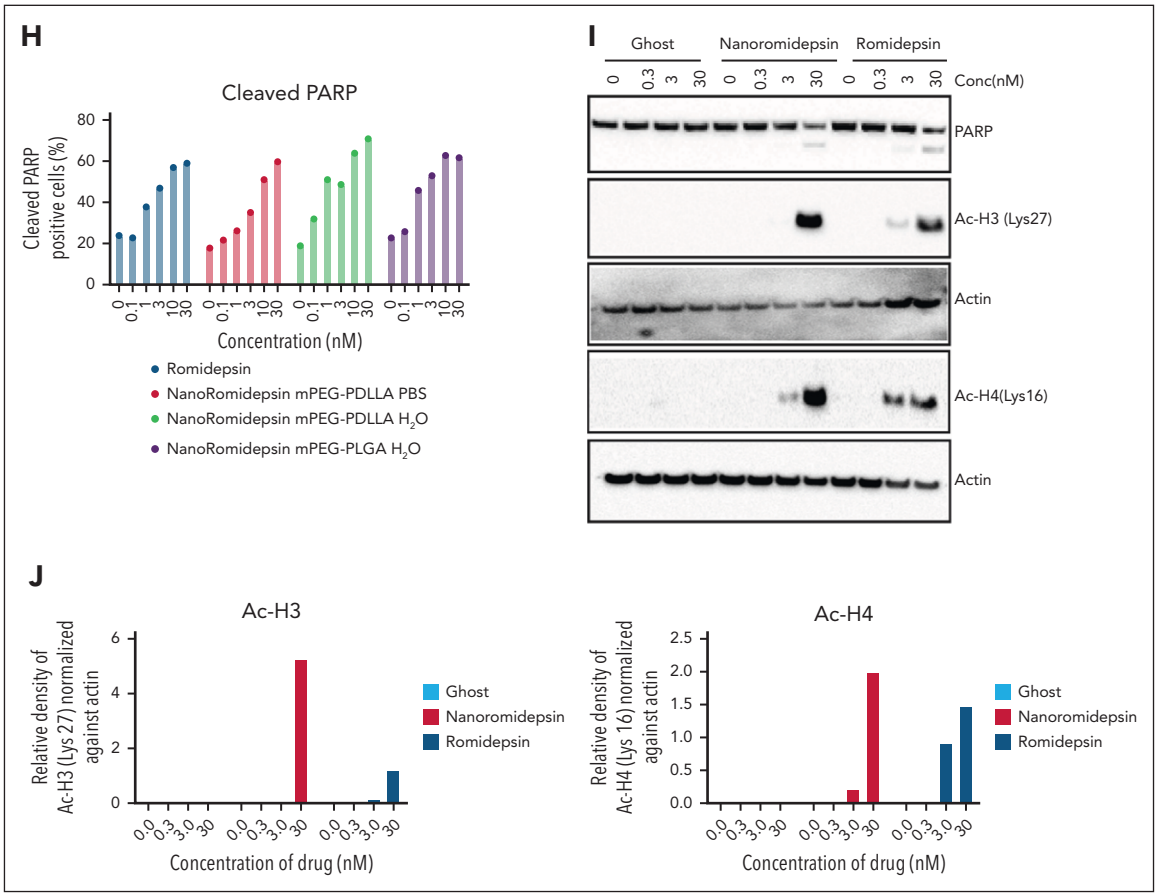

Figure 1 (continued) nanoromidepsin analogs manufactured using combinations of different polymers (PDLLA and PLGA) and solvents (PBS and H_2O). The cytotoxicity was determined using CellTiter-Glo assay after 60 hours of treatment. (F) IC_{50} (nanomolar) for romidepsin and nanoromidepsin analogs for the 6 cell lines at 60 hours. Flow cytometry of (G) Ac-H3 (Lys27), and Ac-H4 (Lys16) (H) cleaved PARP expressing in HH cell line after 30 hours of treatment with indicated treatment of increasing Conc of romidepsin and nanoromidepsin. Data presented as mean ± standard deviation. (I) Western blot analysis of Ac-H3 (Lys27), Ac-H4 (Lys16), and cleaved PARP at 24 hours after treatment with ghost, romidepsin, and nanoromidepsin mPEG-PDLLA H_2O; and (J) densitometry analysis of the western blot analysis. Ac-H3, acetylated histone 3; Ac-H4, acetylated histone 4; Conc, concentration; MFI, mean fluorescence intensity; ZP, zeta potential.

was similar to romidepsin (IC_{50} = 0.6-1.9 nM; Figure 1F). Both nanoromidepsin mPEG-PDLLA PBS (IC_{50} = 1.3-7.5 nM) and nanoromidepsin mPEG-PLGA H_2O (IC_{50} = 1.1-5.5 nM) were slightly less potent. There was no growth inhibition of any cell line with the corresponding ghost PNP lacking romidepsin (supplemental Figure 1). We used flow cytometry to identify early chromatin remodeling events and apoptosis, and western blotting to assess later-stage pathway alterations. Flow cytometry and western blotting demonstrated that treatment with all 3 romidepsin PNPs induced apoptosis similar to romidepsin as shown by increased levels of cleaved poly(ADP-ribose) polymerase (PARP) (Figure 1H-I).

A concentration-dependent increase in H3/H4 acetylation was observed by flow cytometry with romidepsin or 1 of the 3 romidepsin PNPs (Figure 1G). Among the 3 PNPs, the nanoromidepsin mPEG-PDLLA–H_2O PNP was comparable to romidepsin in its pattern of histone acetylation. Western blot analysis demonstrated increased H3/H4 acetylation after exposure to romidepsin or nanoromidepsin mPEG-PDLLA H_2O at 24 hours (Figure 1I-J). Acetylation of H3 and H4 were four-fold and 1.5-fold higher in cells treated with 30 nM nanoromidepsin compared with romidepsin (24 hours).

Between nanoromidepsin mPEG-PLGA and mPEG-PDLLA, nanoromidepsin mPEG-PDLLA exhibited superior physicochemical properties (size, PDI, and encapsulation efficiency), the lowest IC_{50}, and comparable histone acetylation and PARP cleavage compared with romidepsin (Figure 1E-J). This prompted further optimization, scale up, physicochemical characterization, and interrogation of its in vitro activity (supplemental Figure 2A-C,E-G).

Nanoromidepsin exhibited superior cytotoxicity against primary LGL leukemia samples

Although romidepsin has not been clinically used in large granular lymphocyte (LGL) leukemia, this disease model serves to explore nanoromidepsin's effects across T-cell malignancies. Romidepsin and nanoromidepsin were compared using samples from patients with LGL leukemia. Nanoromidepsin demonstrated superior cytotoxicity in TL-1 (a T-cell LGL) and NKL (a natural killer–cell LGL) cell lines (supplemental Figure 3E). An ex vivo cytotoxicity assay performed on peripheral blood mononuclear cells (PBMC) from patients with LGL leukemia demonstrated that nanoromidepsin exhibited a statistically greater potency, (IC_{50}, 3.1 ± 1.7 nM vs IC_{50}, 9.06 ± 5.7 nM; P = .0057; Figure 2A-B). As whole PBMC samples also

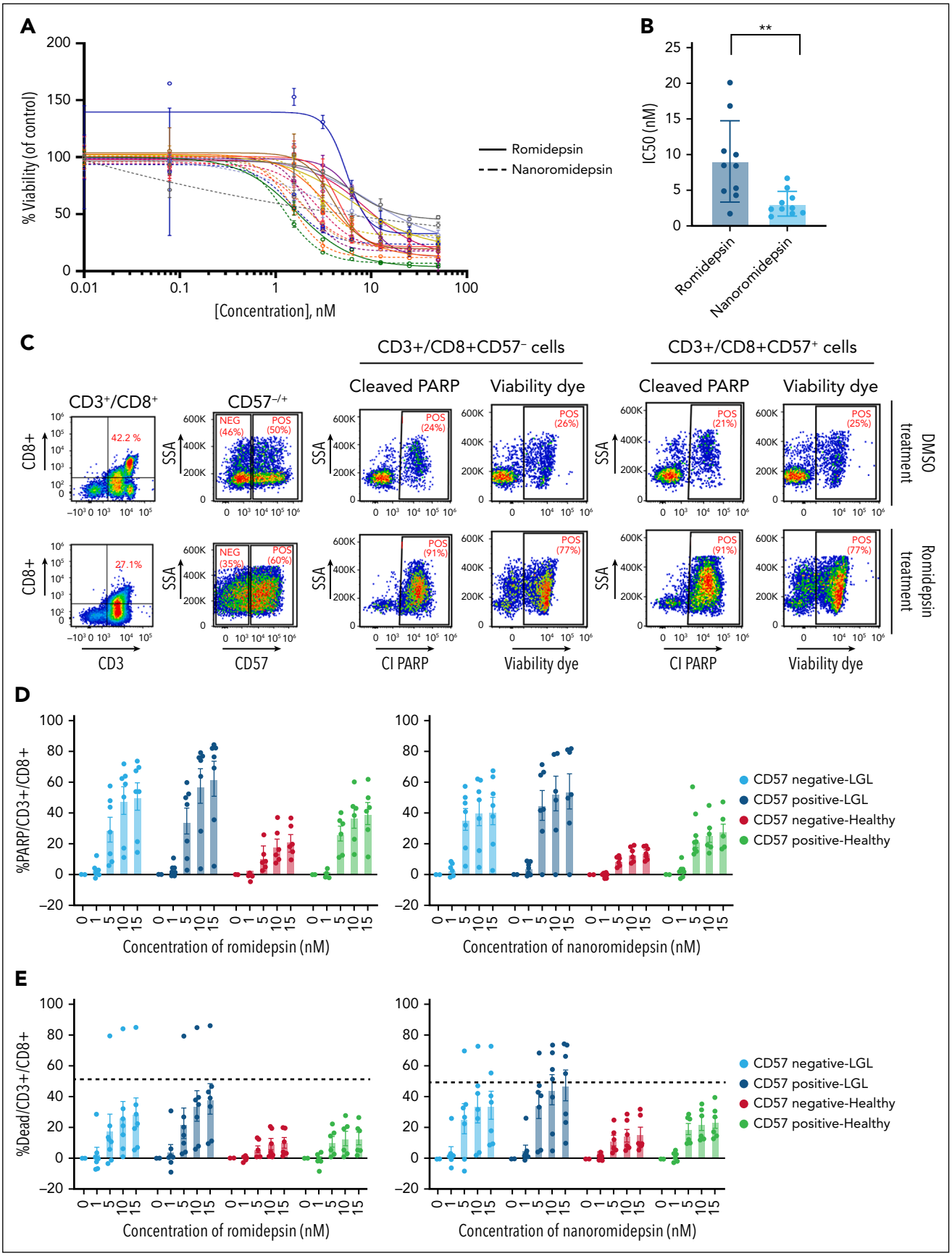
A
% Viability (of control)
[Concentration], nM
Romidepsin
Nanoromidepsin
B
IC50 (nM)
**
Romidepsin
Nanoromidepsin
C
CD3+/CD8+CD57− cells
CD3+/CD8+CD57+ cells
Cleaved PARP
Viability dye
CD3+/CD8+
CD57−/+
CD8+
CD3
SSA
CD57
Cl PARP
42.2 %
27.1%
NEG (46%)
POS (50%)
NEG (35%)
POS (60%)
POS (24%)
POS (26%)
POS (21%)
POS (25%)
POS (91%)
POS (77%)
POS (91%)
POS (77%)
DMSO treatment
Romidepsin treatment
D
%PARP/CD3+/CD8+
Concentration of romidepsin (nM)
Concentration of nanoromidepsin (nM)
CD57 negative-LGL
CD57 positive-LGL
CD57 negative-Healthy
CD57 positive-Healthy
E
%Dead/CD3+/CD8+
Concentration of romidepsin (nM)
Concentration of nanoromidepsin (nM)
CD57 negative-LGL
CD57 positive-LGL
CD57 negative-Healthy
CD57 positive-Healthy

Figure 2.

contain a small proportion of nonleukemic cells, we designed a multicolor flow cytometry–based functional assay[7] to quantify apoptosis in $CD3^+/CD8^+CD57^+$ or $CD3^+/CD8^+CD57^-$ cell populations ($CD8^+$ T-cell markers) of patients with LGL leukemia (Figure 2C). The percentage of $CD3^+/CD8^+CD57^-$ and $CD3^+/CD8^+CD57^+$ cells positive for cleaved PARP was similar for nanoromidepsin- and romidepsin-treated PBMC samples. However, the percentage of dead cells (viability dye positive) in $CD3^+/CD8^+CD57^+$ and $CD3^+/CD8^+CD57^-$ populations was quantitatively higher in the nanoromidepsin-treated samples. Although the difference was not statistically significant ($P = .59$ and .46, respectively; Figure 2D-E).

Nanoromidepsin demonstrates superior PK parameters and biodistribution compared with romidepsin

The PK profiles of nanoromidepsin and romidepsin were compared in BALB/c mice by quantifying plasma romidepsin concentrations after IV or IP administration. Irrespective of the route of administration, the plasma concentration of free romidepsin rapidly declined after 6 hours (Figure 3A). Nanoromidepsin exhibited a higher area under the curve (AUC) of exposure 48 hours after treatment, irrespective of the route of administration. After IV administration, the peak concentration (C_{max}), half-life, and AUC for nanoromidepsin were 10-, 1.5-, and 25-fold higher compared with free romidepsin, respectively (Table 1). The PK analyses suggested that the clearance of romidepsin was faster after IV compared with IP administration. The peak concentrations achieved after IP administration of nanoromidepsin and romidepsin were 804 and 218 nM, respectively. After IV administration, the peak concentrations of nanoromidepsin and romidepsin were 425 and 38 nM, respectively. Based on the in vitro data across the TCL cell lines studied, the IC_{50} of nanoromidepsin PDLLA was around 2 to 8 nM (supplemental Figure 2F). Collectively, these data suggest that nanoromidepsin achieves a concentration 50- to 400-fold greater than the IC_{50} of romidepsin with a dose that was only one-half of the MTD of nanoromidepsin (Figure 3A).

To characterize the biodistribution of nanoromidepsin, time-dependent tissue and tumor uptake studies were performed. H9-dTomato-Luc xenograft mice were administered with nanoromidepsin coencapsulated with DiO (supplemental Figure 2D). Whole-body fluorescence imaging demonstrated that the fluorescence signal of nanoromidepsin-DiO–treated mice was greater compared with the free DiO-treated mice (Figure 3B-C). Ex vivo imaging of the organs showed that nanoromidepsin selectively accumulated in the tumor at 72 hours after administration. Modest uptake was observed in the liver only in free DiO-treated mice (Figure 3D). Quantification of fluorescent signal in harvested organs showed a significant ($P < .05$) accumulation of nanoromidepsin-DiO in the tumor compared with the free DiO (Figure 3E). In a complementary assay, H9-dTomato-Luc engrafted mice were injected with 4 mg/kg romidepsin or nanoromidepsin. Quantitation of romidepsin in the tumor at 24 hours after administration revealed an intratumoral concentration of romidepsin in the romidepsin- and nanoromidepsin-treated groups of 3.57 and 45.8 ng/mg of protein, respectively. These data demonstrate a substantially greater accumulation of the romidepsin in tumor tissue of nanoromidepsin-treated animals (Figure 3F). Increased accumulation was observed in the liver, spleen, and lungs after nanoromidepsin administration, consistent with clearance via the mononuclear phagocyte system, with no drug detected in the heart. Importantly, no evidence of organ-specific toxicity was observed (supplemental Figure 7).

Nanoromidepsin exhibits superior tolerability compared with romidepsin in vivo

The safety and tolerability of nanoromidepsin were determined in a single-dose toxicity study with escalating doses of nanoromidepsin or romidepsin (IP and IV) to identify the MTD in BALB/c mice. Changes in body weight and clinical score were assessed as a function of time and dose. Although mice in both treatment cohorts experienced weight loss after treatment, body weight returned to pretreatment levels in most animals after 15 days (Figure 4A-B; supplemental Figure 3). Mice treated with 8 mg/kg IP of either romidepsin or nanoromidepsin met criteria for euthanasia 3 days after treatment. At this level, 80% of the mice treated with romidepsin were dead 3 days after treatment, compared with 40% with nanoromidepsin. This established the MTD for both drugs by IP (5 mg/kg). In the IV cohorts, 10 mg/kg was the highest dose explored for both drugs. Mice lost ~15% body weight within 3 days after treatment with either drug, although all mice in both treatment groups recovered after 15 days. Escalation beyond 10 mg/kg was technically not feasible given the volume of the IV dose required at the available nanoromidepsin concentration.

Although the AUC and C_{max} of nanoromidepsin were considerably higher when drug was administered IP vs IV (Figure 3A), a study in H9-dTomato-Luc xenograft confirmed that the IP administration route for nanoromidepsin induced unacceptably high toxicity (supplemental Figure 4). These findings were consistent with the literature suggesting that many nanoparticles cannot be administered safely by the IP route given the association with peritonitis likely due to the physical features of the particle.[8] For these reasons, all subsequent in vivo studies used only the IV route.

Multidose studies were conducted in H9-dTomato-Luc xenograft-containing NSG mice (supplemental Table 1; supplemental Figures 5 and 6), approximating the single-agent dose intensity and corresponding to one-fourth, one-half, and three-fourths of the MTD for nanoromidepsin. Repeat dosing

Figure 2. Effect of nanoromidepsin on PBMC samples from patients with primary LGL leukemia. (A) Freshly frozen PBMCs from patients with LGL leukemia were treated with indicated doses of romidepsin (solid line) or nanoromidepsin (dotted line) for 48 hours. (B) IC_{50} (nanomolar) for romidepsin and nanoromidepsin for 10 patients with LGL leukemia at 48 hours. (C) PBMCs from patients with LGL leukemia and healthy donor as a control were screened by flow cytometry. The lymphocyte and singlet cell gating were performed as described earlier. The $CD3^+/CD8^+CD57^{+/-}$ cells were gated from singlet lymphocyte population as indicated. The cleaved PARP or viability dye staining was analyzed in $CD3^+/CD8^+CD57^+$ or $CD3^+/CD8^+CD57^-$ cells as indicated. The flow images were generated from a representative PBMC sample from a patient with LGL (patient 03), treated with DMSO or romidepsin (10 nM). Ghost or nanoromidepsin-treated samples were similarly analyzed. (D) Cleaved PARP (apoptosis) and (E) live-dead dye staining (cell viability) after the incubation with romidepsin and nanoromidepsin for 48 hours. Data presented as percentage $CD3^+/CD8^+CD57^+$ (more differentiated LGL) or $CD3^+/CD8^+CD57^-$ (less differentiated LGL) cells positive for cleaved PARP or live-dead dye staining. The data presented after subtracting spontaneous apoptosis or cell viability values from the DMSO-treated controls. CI PARP, cleaved PARP; DMSO, dimethyl sulfoxide; NEG, negative; POS, positive.

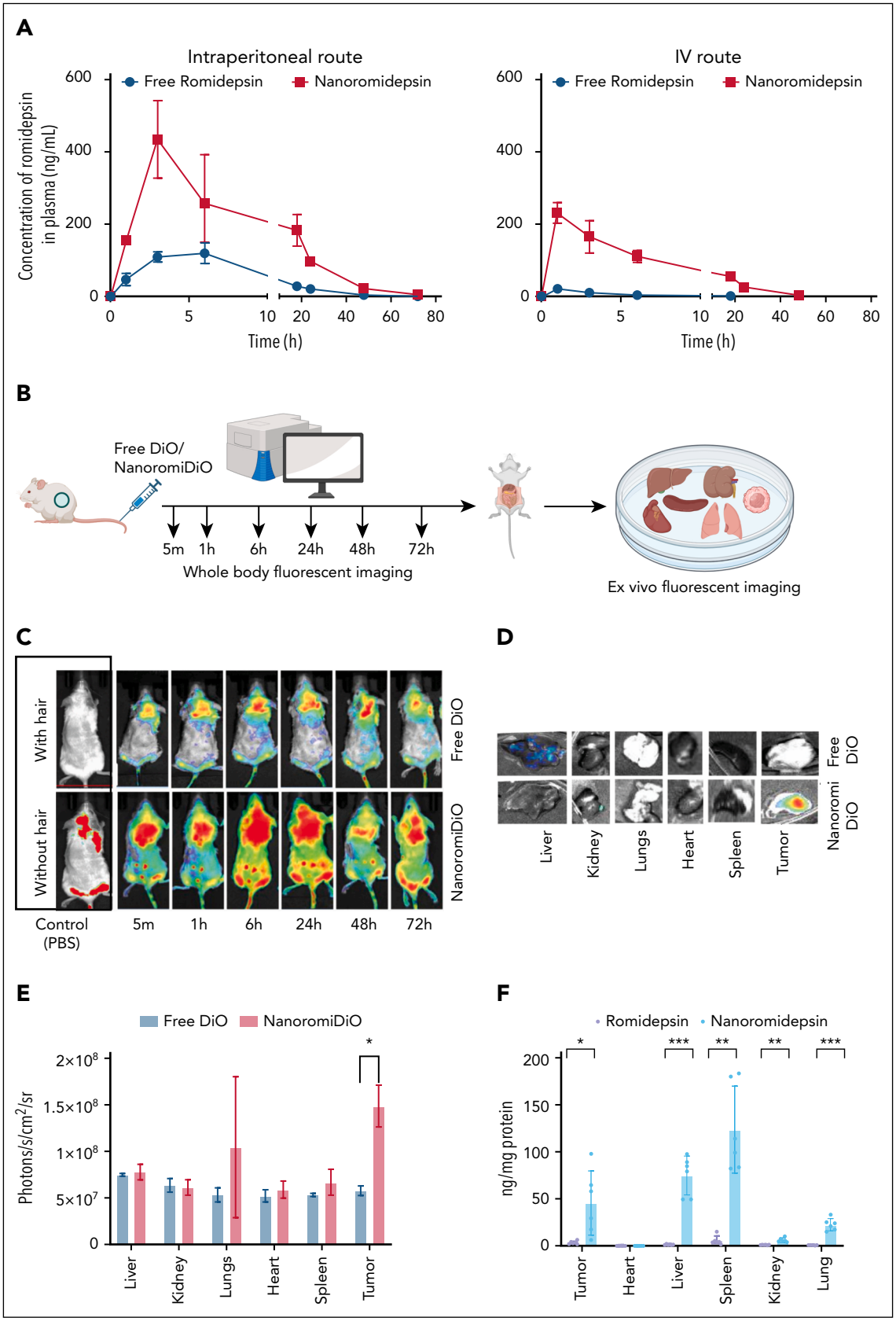

Figure 3. PKs and tissue distribution of nanoromidepsin in vivo. (A) Plasma concentration-time dependence plot of romidepsin concentration in plasma after IP or IV administration of a single treatment with romidepsin or nanoromidepsin. (B) Diagram representing experimental time points associated with nanoromidepsin coloaded with a fluorescent dye DiO or free DiO administration, fluorescent images evaluation, and organs collection. (C) Fluorescence images of H9-dTomato-Luc tumor-bearing mice taken at different time points after IV injection of free DiO or DiO and romidepsin-encapsulated nanoparticle (NanoromiDiO). Ex vivo fluorescence images (D) and

Table 1. PK parameters of romidepsin and nanoromidepsin after IP and IV route of administration

Route of administration		IP			IV		
Parameter	Unit	Free romidepsin	Nanoromidepsin	Fold change (nano/free)	Free romidepsin	Nanoromidepsin	Fold change (nano/free)
$T_{1/2}$	h	9.8	11.6	1.2	5.2	7.6	1.5
T_{max}	h	6.0	3.00	2	1.00	1.00	
C_{max}	ng/mL	119.9	434.7	3.6	21.3	231.0	10.8
AUC_{0-t}	ng*h/mL	1918.9	6939.9	3.6	99.2	2532.1	25.5

AUC_{0-t}, the AUC up to the last quantifiable time point; C_{max}, maximum plasma concentration; nano, nanoromidepsin; nano/free, nanoromidepsin/free romidepsin; T_{max}, time to maximum plasma concentration; $T_{1/2}$, half-life.

studies revealed that romidepsin produced a higher degree of weight loss (>10%) and clinical score (>3) compared with nanoromidepsin at equivalent dose. The most tolerated dose and schedule of nanoromidepsin was identified to be 4 mg/kg once weekly for 3 weeks (Figure 4C-D). Romidepsin at a dose of 8 mg/kg demonstrated acute toxicity leading to death of all mice (thus lethel dose, 50% [LD50] is significantly less than 8 mg/kg) within 4 days, whereas 8 mg/kg nanoromidepsin was lethal in only 50% of mice, representing the LD50 of nanoromidepsin (Figure 4E-F).

To assess tissue-specific toxicity, liver and tumor were assessed for histopathology (Figure 4G). Liver sections from all cohorts exhibited normal microarchitecture without any indication of inflammation or necrosis. Although there were no signs of drug-induced toxicity in the liver sections of either treatment cohort, the LC-MS quantification confirmed that the concentrations of romidepsin in the liver were substantially less with nanoromidepsin compared with romidepsin (13.18 and 46.68 ng/mg of protein, respectively; $P < .0009$; Figure 4H). Tumor sections from the mice treated with the ghost PNP revealed sheet-like infiltrates of large, atypical lymphocytes with pleomorphic nuclei, distinct nucleoli, and amphophilic cytoplasm, consistent with viable tumor. The romidepsin- and nanoromidepsin-treated tumor sections showed varying degrees of treatment-related necrosis, with no substantial difference in histopathology between the treatment groups. The mean plasma concentrations of romidepsin at 1 and 24 hours following 3 consecutive treatments of romidepsin (weekly doses for 3 weeks) were 51 and 4.9 ng/mL (Figure 4I). These data indicate a rapid decline in mean plasma concentration, implying a rapid clearance of romidepsin from the blood. In contrast, the mean plasma concentrations of romidepsin in the plasma collected at 1 and 24 hours following the same dose of nanoromidepsin were 120.3 and 40.7 ng/mL (2.3- and 8.3-fold greater than the free romidepsin).

Nanoromidepsin shows superior activity and a survival advantage in murine xenograft models

To determine differences in efficacy, H9-dTomato-Luc xenograft-engrafted mice were treated with 3.5 mg/kg weekly for 3 weeks with romidepsin or nanoromidepsin (Figure 5A). After 3 treatments, the cohort receiving romidepsin exhibited moderate antitumor activity, with tumor growth inhibition assessed by BLI of 54% and 57% compared with the vehicle and ghost PNP cohorts, respectively ($P = .0315$ vs vehicle; $P = .04$ vs ghost PNP). Nanoromidepsin inhibited tumor growth by 90% and 91% compared with the vehicle and ghost PNP cohorts, respectively ($P = .0003$ vs vehicle; $P = .0019$ vs ghost PNP). Although there was no statistically significant difference in the growth delay observed between romidepsin and nanoromidepsin ($P = .6665$), the nanoromidepsin cohort demonstrated greater tumor reduction by BLI compared with romidepsin after 3 weeks of treatment (Figure 5B). The tumor BLI signal was reduced 1 week after the first treatment, which held constant for the next 3 weeks for both treatment cohorts (Figure 5B,D-E), supporting nanoromidepsin's superiority. Mice treated with nanoromidepsin or romidepsin showed no statistically significant survival benefit at this dose, which may be due to cytokinetic failures resulting from compromised dose intensity (Figure 5C).

In response to the insignificant survival benefit as observed in Figure 5 likely due to the low dose and short treatment time, we administered both drugs on a 35-day cycle at 4 mg/kg per week for 4 consecutive weeks (Figure 6A). Significant toxicity was noted after 1 cycle with romidepsin. A consistent increase in the BLI was observed in the PBS, ghost PNP, and romidepsin-treated mice cohort until day 24 (Figure 6B-C). A growth delay was observed in the nanoromidepsin cohort. Moreover, 33% of mice died after 3 weeks of treatment with romidepsin, whereas treatment with nanoromidepsin resulted in no deaths (Figure 6C). Nanoromidepsin resulted in a statistically significant prolongation in OS compared with romidepsin (Figure 6D). The OS in the control, ghost PNP, and romidepsin-treated mice was 38 days (for all 3 groups), compared with 53 days with nanoromidepsin ($P < .001$). We did observe some toxicity after the third treatment in cycle 2, suggesting that perhaps a lower maintenance dose might be worth exploring in the future. These data demonstrate superior biological activity, efficacy, and survival benefit of nanoromidepsin compared with romidepsin.

Figure 3 (continued) corresponding fluorescence intensity (E) of tumor and major organs (tumor, liver, spleen, kidney, heart, and lung, respectively) dissected at 72 hours after injection. Statistical significance was determined by using Student *t* test (Mann-Whitney): $*P < .05$; $**P < .01$; $***P < .001$. (F) Mice bearing H9-dTomato-Luc xenograft were treated with 4 mg/kg romidepsin and nanoromidepsin. After 24 hours, tumors (n = 6) were collected for LC-MS–based quantification of romidepsin in tumor tissue.

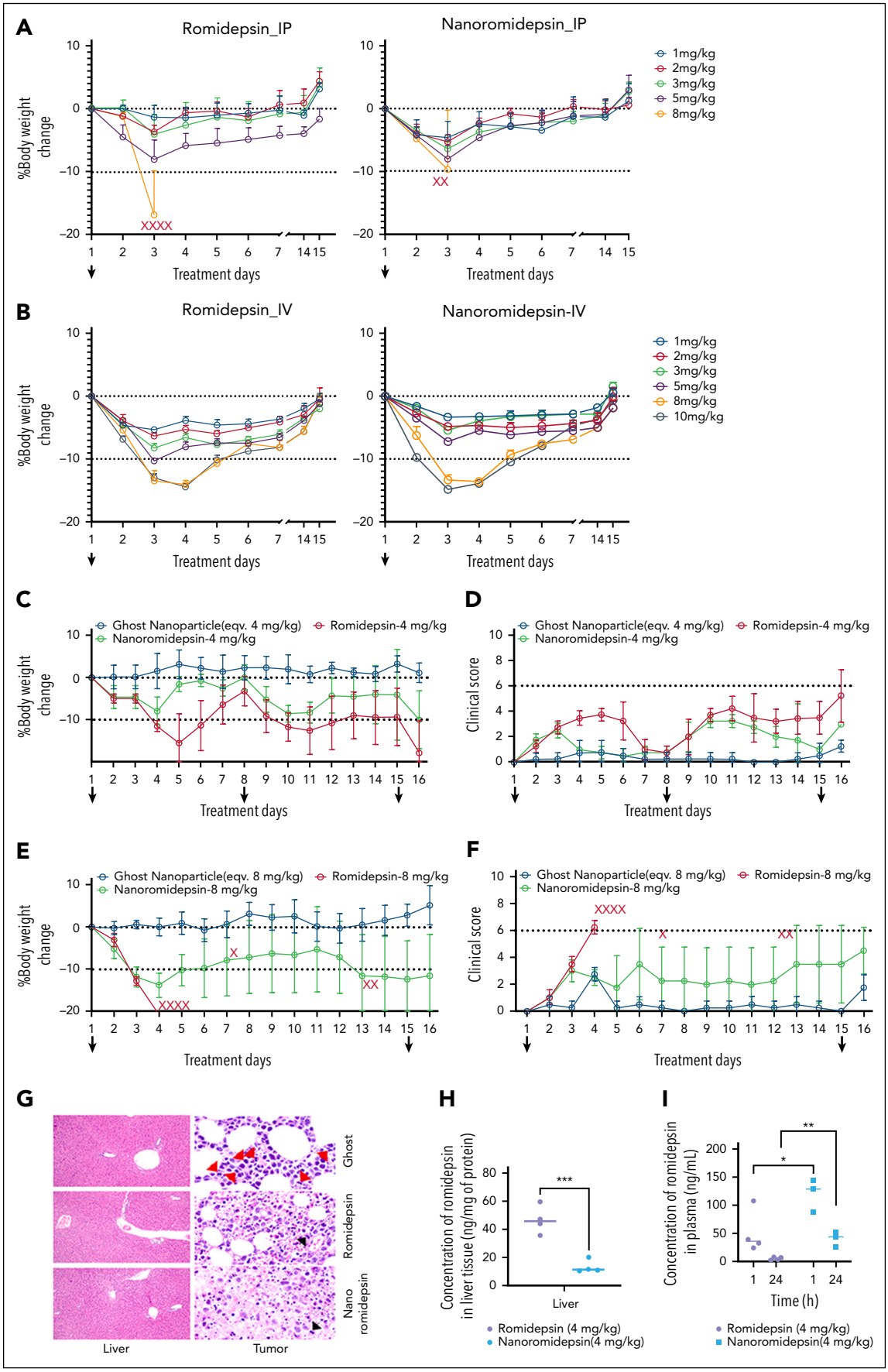
A
Romidepsin_IP
Nanoromidepsin_IP
%Body weight change
Treatment days
1mg/kg
2mg/kg
3mg/kg
5mg/kg
8mg/kg
B
Romidepsin_IV
Nanoromidepsin-IV
10mg/kg
C
Ghost Nanoparticle(eqv. 4 mg/kg)
Romidepsin-4 mg/kg
Nanoromidepsin-4 mg/kg
D
Clinical score
E
Ghost Nanoparticle(eqv. 8 mg/kg)
Romidepsin-8 mg/kg
Nanoromidepsin-8 mg/kg
F
G
Ghost
Romidepsin
Nano romidepsin
Liver
Tumor
H
Concentration of romidepsin in liver tissue (ng/mg of protein)
Liver
Romidepsin (4 mg/kg)
Nanoromidepsin(4 mg/kg)
I
Concentration of romidepsin in plasma (ng/mL)
Time (h)

Figure 4.

Discussion

The dwindling options to treat patients with R/R PTCL has created an urgent need to rethink how we develop new drugs for challenging orphan diseases. In the United States, pralatrexate and belinostat are the only drugs still approved for patients with R/R PTCL, albeit they are not full approvals. Loss of the romidepsin indication in R/R PTCL has put physicians and patients in a challenging position. With few new drugs emerging, improving existing treatments or developing new ones through combinatorial regimens offers a relatively low-risk way to advance care.

Romidepsin in combination with other epigenetically targeted drugs such as the DNA methyltransferase (DNMT) inhibitor 5-azacytidine appears to produce the best overall response rate and PFS data of any drug or drug combination to date in this population.[9,10] These clinical and preclinical experiences suggest that combinations with an HDACi, romidepsin being among the most potent, may represent 1 straightforward path to create new treatment platforms for this population.[11,12] Although preclinical data highlight romidepsin's superior potency compared with other HDACis clinically, romidepsin produces an overall response rate of 25%, a PFS of 3 to 4 months, and a median response duration >1 year, all disappointing results given the preclinical findings. This discrepancy may stem from its suboptimal pharmacologic properties, including high protein binding (92%-94%), a short half-life (3.8 hours), and limited volume of distribution (Vd; 44.5 L), which constrain its effects on transcriptional activation.[13,14]

Pharmacologic optimization offers a path to overcome the intrinsic limitations of therapeutic agents, and PNPs offer the prospect of resolving the liabilities associated with suboptimized drugs.[15] The amphiphilic diblock lactides used to make PNP are considered biocompatible, biodegradable, and nontoxic, which enhances their elimination, improves their tolerability, and reduces their immunogenicity.[16] The inclusion of the PEG chain to the PNP has been shown to reduce the elimination of the particles via the host immune system, maximizing circulation time.[17] An attractive feature of this platform is that hydrophobic drugs can be readily incorporated and even conjugated to the polymer.[18-20] In our case, PEGylation likely protects romidepsin by forming a hydrophilic barrier that blocks external reducing agents such as glutathione and serum thiols, stabilizing romidepsin's oxidized disulfide state while preventing premature reduction. In addition, PNPs typically have a size of <100 nm, which aids in improving the Vd, allowing for a bioconcentration of drug in tissue, particularly tumor. Herein, we exploited the unique physicochemical properties of a tailored PNP, including optimal size and surface properties, enhanced Vd, and augmented tumor bioavailability, in an effort to address the limitations of "naked" romidepsin. The goal was to enhance the epigenetic effects of the drug deploying a scalable translational approach.[21-23] We designed our PNPs to be ~50 nm, which has been suggested to be a feature that favors bioconcentration in the tumor microenvironment.[24] The bioluminescent in vivo assay that deployed a PNP containing both romidepsin and DiO clearly established a predilection for the PNP to bioaccumulate in the tumor microenvironment. Although several mechanisms can explain this, porous and leaky vasculature have been advanced as one of the major explanations.[25-30]

In patients with PTCL, administration of romidepsin (14 mg/m^2 IV over 4 hours on days 1, 8, and 15 of a 28-day cycle) yields a C_{max} and total AUC ($AUC_{0-\infty}$) of 377 ng/mL and 1549 ng*h/mL, respectively. In rats, single slow IV bolus of romidepsin administration (0.33 and 0.67 mg/kg) achieved a mean AUC_∞ of 10.3 and 18.1 ng*h/mL, respectively.[31] After a single IV dose of romidepsin and nanoromidepsin, the C_{max} in BALB/c mice was 21.3 and 231.0 ng/mL, respectively. Another major difference was seen in the AUC, which was 99.2 and 2532.1 ng*h/mL for romidepsin and nanoromidepsin, respectively. Nanoromidepsin exhibited a 1.5-fold increase in half-life compared with romidepsin, indicating prolonged availability in plasma. Recognizing all the cross-species differences, these data suggest that nanoromidepsin in these murine models approximated or dramatically exceeded those PK parameters established in humans, which is also supported by our biodistribution study, in which PNP was shown to preferentially bioaccumulate in tumor. Some conventional polymeric nanoparticles have been shown to accumulate in organs such as the spleen, liver, and kidneys, potentially limiting their therapeutic potential.[17] This is important as we observed similar findings after a short-term treatment, though the BLI imaging confirmed selective bioaccumulation of nanoromidepsin at later time points in tumor. These findings are concordant with previous studies indicating that a PNP tailored for the active pharmaceutical ingredient can improve bioavailability, thereby optimizing mechanism of action,[32,33] a factor that may be especially important for drugs targeting the epigenome.

The improvement in the PK parameters raises concerns about incrementally worse tolerability. In a series of comprehensive single- and repeat-dose toxicity studies, nanoromidepsin was found to be substantially safer than romidepsin, even at the highest doses studied. These data have established a sound basis to identify the MTD, optimal route of administration, and acceptable dosing schedule prior to the efficacy studies. Our in vivo toxicity assays affirmed that nanoromidepsin was safer compared with romidepsin, and exhibited less accumulation in the liver as shown in biodistribution studies and as supported

Figure 4. Tolerability of romidepsin and nanoromidepsin in vivo. BALB/c mice were administered a single dose of romidepsin or nanoromidepsin IP (A) and IV (B). Tolerability was assessed by monitoring body weight and overall health conditions. X represents dead mice; H9-dTomato-Luc xenograft-bearing NSG mice were administered 4 mg/kg of romidepsin or nanoromidepsin by IV or IP for arrow indicated days (1, 8, and 15 days). (C) Percentage of body weight changes as function of starting weights (±standard error of the mean [SEM]) are shown; (D) clinical score. H9-dTomato-Luc xenograft-bearing NSG mice administered with 8 mg/kg of romidepsin or nanoromidepsin by IV for arrow indicated days. Depicted are percentage of body weight changes as function of starting weights (±SEM) (E); clinical score (F). (G) Liver and tumor were harvested, fixed in formalin for pathological analysis after hematoxylin and eosin (H&E) staining, and processed for LC-MS–based quantification of romidepsin. H&E staining of hepatic parenchyma from ghost, romidepsin-, and nanoromidepsin-treated mice (original magnifications ×200). Soft tissue tumors from ghost-treated mice showed pleomorphic nuclei and brisk mitosis (original magnification ×1000). Romidepsin- and nanoromidepsin-treated tumors associated with varying treatment-related necrosis (original magnifications ×1000). Red and black arrows indicate mitotic figures and necrosis/apoptosis. (H) LC-MS–based quantification from liver. (I) Blood was collected by submandibular bleeding after 1 and 24 hours after the last treatment with 4 mg/kg romidepsin and nanoromidepsin in the repeat-dose study. Plasma was collected and the romidepsin was quantified. LC-MS–based quantification of plasma collected from the experiment described in panel C after 1 and 24 hours. Statistical significance was determined by using Student *t* test (Mann-Whitney): $*P < .05$; $**P < .01$; $***P < .001$.

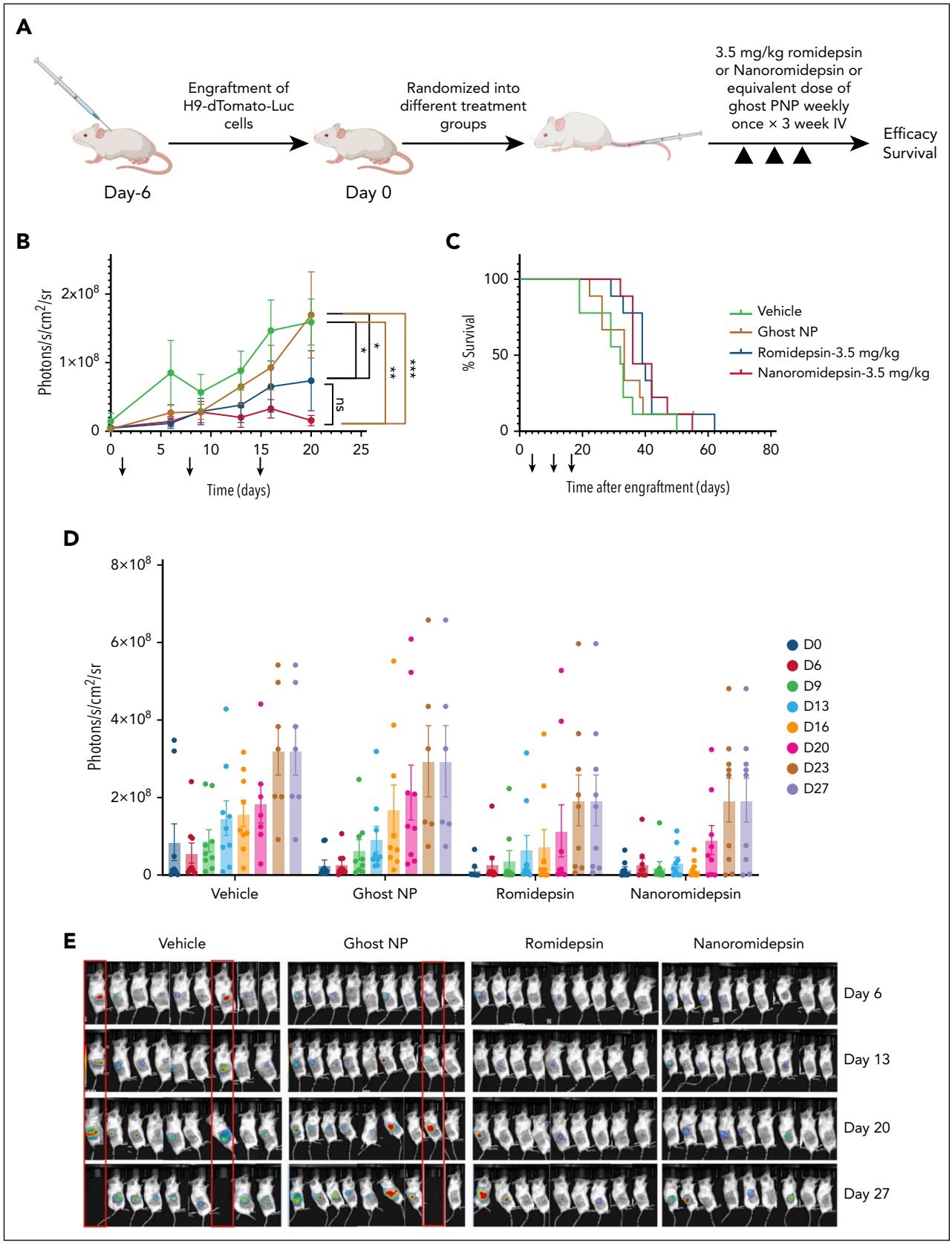

Figure 5. Nanoromidepsin showed superior activity but similar survival rate compared with romidepsin in TCL xenograft-bearing NSG mice. (A) Diagram representing the inoculation and dosing schedule of romidepsin and nanoromidepsin in H9-dTomato-Luc xenograft-bearing mice. (B,D) Region-of-interest analysis of BLIs (readout for tumor growth) from different treatment groups were recorded at various time points over the course of 8 weeks. Statistical significance was determined by using Student *t* test (Mann-Whitney): $^{*}P < .05$; $^{**}P < .01$; $^{***}P < .0001$. (C) Survival curves for romidepsin-treated, nanoromidepsin-treated, ghost NP and control mice (n = 9 per group). The arrows indicate treatment days. Statistical significance was determined by using log-rank test: $^{*}P < .05$; $^{**}P < .01$; $^{***}P < .001$. (E) Whole-body bioluminescence images of H9-dTomato-Luc xenograft-bearing mice taken at the indicated day. Red box indicates dead mouse. NP, nanoparticle; ns, not significant.

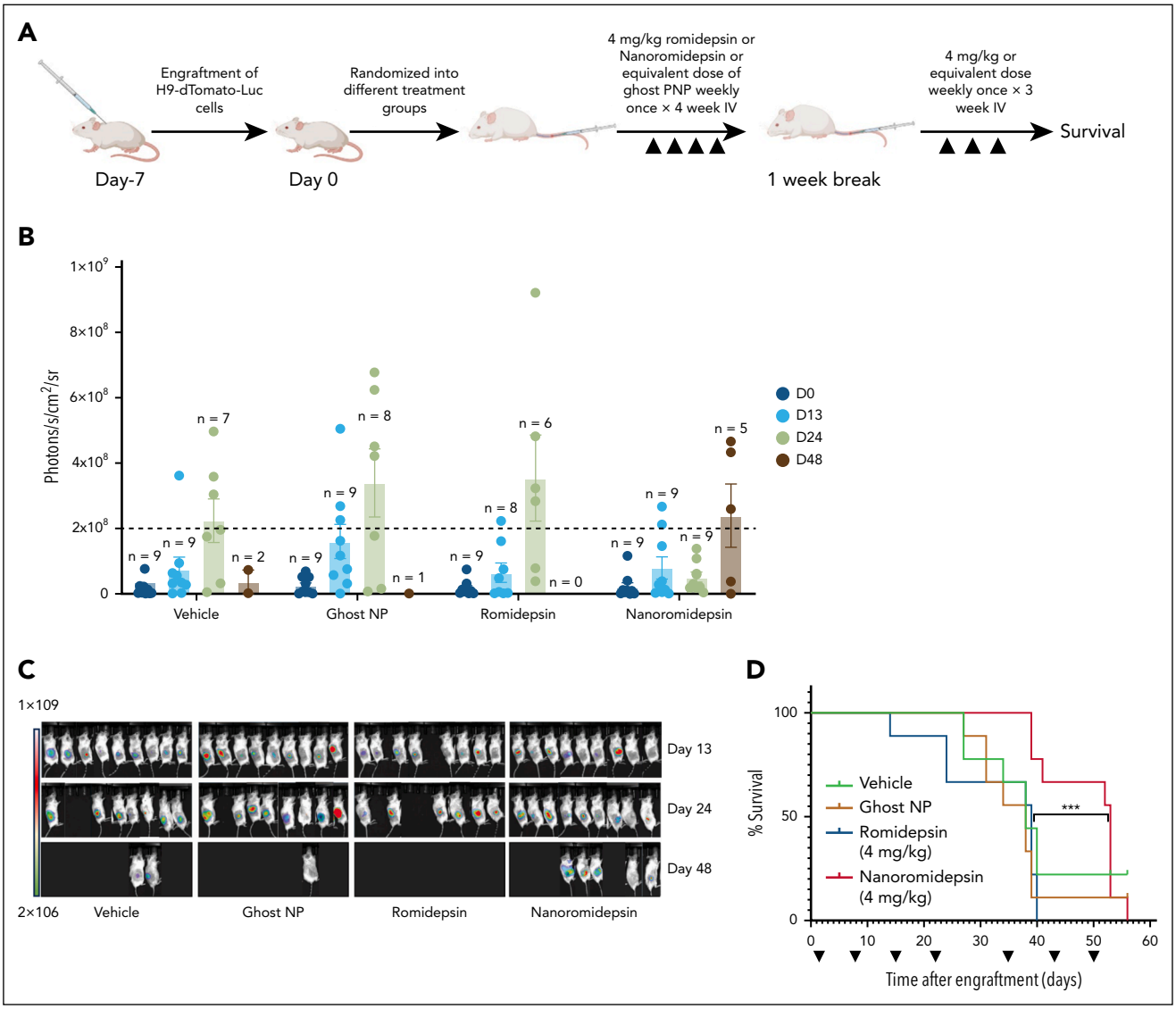

Figure 6. Dosing schedule change of romidepsin-encapsulated NP showed superior activity and survival rate compared with romidepsin in CTCL xenograft-bearing NSG mice. (A) Diagram representing the inoculation and dosing schedule of romidepsin and nanoromidepsin in TCL xenograft-bearing mice. (B) Region-of-interest analysis of BLIs (readout for tumor growth) from different treatment groups at various time points during the course of treatment and plotted as bar graph. (C) Whole-body bioluminescence images of H9-dTomato-Luc xenograft-bearing mice taken at the indicated day. (D) Survival curves for romidepsin-treated, nanoromidepsin-treated, ghost NP, and control mice (n = 9 per group). The arrows indicate treatment days. Statistical significance was determined by using log-rank test: **P* < .05; ***P* < .01; ****P* < .001.

by the histopathology and LC-MS–based quantification of drug in vital organs. In the xenograft models, nanoromidepsin exhibited an LD50 value of 8 mg/kg, compared with 5 mg/kg for romidepsin (Figure 4E; supplemental Figure 6). The direct comparison of body weight loss and clinical toxicity scores in mice confirmed the superior safety profile of nanoromidepsin at all doses and schedules studied.

Across all efficacy studies, nanoromidepsin dosed at 4 mg/kg weekly for 4 consecutive weeks followed by retreatment produced substantially superior growth delay, and an OS advantage compared with romidepsin. An OS advantage is based on the depth of a complete remission. In clinical practice, durable remissions are often achieved with multiple cycles of combination therapy. The improved tolerability and efficacy of nanoromidepsin would suggest that combinations of drugs with nanoromidepsin will further deepen the complete remission, likely translating into improved outcomes for patients with PTCL.

In summary, we have pioneered the development of a unique epigenetically targeted PNP, which exhibits superior PK features, tolerability, and efficacy compared with the historically approved drug. This study represents the first to interrogate the merits of a PNP platform into the pharmacology of an epigenetically targeted drug for these diseases. Future studies will address the mechanisms that account for the bioaccumulation of the romidepsin PNP in the tumor microenvironment, as well as the differences in gene expression and how this might explain the potent efficacy advantage for nanoromidepsin. We believe the platform has created an opportunity to reconfigure the traditional treatment paradigms for

patients with PTCL, as we now poise this drug for future clinical studies.

Acknowledgments

The authors acknowledge Jeremy Gatesman, Joshua Tennant, and Susan Walker for their technical support. The authors acknowledge Molecular Immunologic & Translational Sciences Core for animal work, Metabolomics Core for nanoparticle characterization, and Flow Cytometry Core facilities.

O.A.O. is grateful for the American Cancer Society Professorship. O.A.O. is funded, in part, by grant 1R01FD006814-01 from the US Food and Drug Administration. The authors are indebted to the Scarlet Feather Foundation support for the Translational Orphan Blood Cancer Research Initiative (TOBCRI) and the Ivy Foundation for their continued support. The authors thank University of Virginia Large Granular Lymphocyte (LGL) Leukemia Registry personnel for their support of this study. The registry was supported by the Bess Family Charitable fund and a gift from a generous anonymous donor (T.P.L. Jr). The data for this study generated in the University of Virginia Flow Cytometry Core Facility (RRID: SCR_017829) and the liquid chromatography-mass spectrometry (LC-MS) work by T.E.F. were partially supported by the National Cancer Institute, National Institutes of Health grant (P30-CA044579).

The funders had no role in the design of the study; in the collection, analyses, or interpretation of data; in the writing of the manuscript; or in the decision to publish the results.

This article is dedicated to the memory of Mark Kester, a colleague, friend, and pioneer in the field of nanochemistry.

Authorship

Contribution: I.P., A.I., T.P.L. Jr, D.J.F., and O.A.O. conceptualized the study; I.P., A.I., M.E.D.-B., A.J., J.S.M., T.M.D., E.M., A.S., D.P.D., S.Z., T.E.F., K.D.J., J.K., and O.A.O. developed the methodology; I.P., A.I., J.W.C., T.E.F., J.K., and O.A.O. were responsible for the investigation; I.P. and J.W.C. were responsible for the visualization; T.P.L. Jr and O.A.O. acquired the funding; I.P. and O.A.O. administered the project; D.J.F. and O.A.O. supervised the study; I.P., A.I., and O.A.O. wrote the original draft of the manuscript; and I.P., A.I., D.P.D., S.Z., J.W.C., D.J.F., K.D.J., and O.A.O. reviewed and edited the manuscript.

Conflict-of-interest disclosure: O.A.O. has received consulting fees and/or stock options from Myeloid Therapeutics and Dren Bio as a member of their scientific advisory board; and research support for a clinical trial from Bristol Myers Squibb (BMS). D.J.F. has received research funding, honoraria, and/or stock options from AstraZeneca, Dren Bio, Recludix Pharma, and Kymera Therapeutics. T.P.L. Jr has received consultancy fees, honoraria, and/or stock options from Keystone Nano, Flagship Labs 86, Dren Bio, Recludix Pharma, Kymera Therapeutics, and Prime Genomics. J.W.C. has received honoraria from BeiGene, and consultancy fees and expert testimony from Bayer. E.M. reports research funding from Merck, Celgene/BMS, Dren Bio, Kyowa Kirin, Vittoria Biotherapeutics, Acrotech, and Everest Clinical Research. A patent has been filed ("Treatment of cancer and autoimmune disorders using nano polymers of histone deacetylase inhibitors"; application publication/patent number: WO2023064634A1; publication date: 20 April 2023). The remaining authors declare no competing financial interests.

ORCID profiles: A.I., 0000-0001-7398-3181; A.S., 0009-0000-3832-5394; D.P.D., 0009-0002-4790-8588; T.E.F., 0000-0001-5170-3951; J.W.C., 0000-0003-1295-3258.

Correspondence: Owen A. O'Connor, University of Virginia Comprehensive Cancer Center, University of Virginia, Charlottesville, VA, 22903; email: owenaoconnor27@gmail.com.

Footnotes

Submitted 13 December 2024; accepted 24 July 2025; prepublished online on *Blood* First Edition 2 September 2025. https://doi.org/10.1182/blood.2024027997.

All data needed to evaluate the conclusions in the study are present in the article and/or the supplemental Materials.

The online version of this article contains a data supplement.

There is a *Blood* Commentary on this article in this issue.

The publication costs of this article were defrayed in part by page charge payment. Therefore, and solely to indicate this fact, this article is hereby marked "advertisement" in accordance with 18 USC section 1734.

REFERENCES

1. Saksouk N, Simboeck E, Déjardin J. Constitutive heterochromatin formation and transcription in mammals. *Epigenetics Chromatin*. 2015;8:3.
2. Bradner JE, West N, Grachan ML, et al. Chemical phylogenetics of histone deacetylases. *Nat Chem Biol*. 2010;6(3):238-243.
3. Glozak MA, Sengupta N, Zhang X, Seto E. Acetylation and deacetylation of non-histone proteins. *Gene*. 2005;363:15-23.
4. Bachy E, Camus V, Thieblemont C, et al. Romidepsin plus CHOP versus CHOP in patients with previously untreated peripheral T-cell lymphoma: results of the Ro-CHOP phase III study (conducted by LYSA). *J Clin Oncol*. 2022;40(3):242-251.
5. Yao Y, Zhou Y, Liu L, et al. Nanoparticle-based drug delivery in cancer therapy and its role in overcoming drug resistance. *Front Mol Biosci*. 2020;7:193.
6. Gagliardi A, Giuliano E, Venkateswararao E, et al. Biodegradable polymeric nanoparticles for drug delivery to solid tumors. *Front Pharmacol*. 2021;12:601626.
7. Jayappa KD, Gordon VL, Morris CG, et al. Extrinsic interactions in the microenvironment in vivo activate an antiapoptotic multidrug-resistant phenotype in CLL. *Blood Adv*. 2021;5(17):3497-3510.
8. Petros RA, DeSimone JM. Strategies in the design of nanoparticles for therapeutic applications. *Nat Rev Drug Discov*. 2010;9(8):615-627.
9. Falchi L, Ma H, Klein S, et al. Combined oral 5-azacytidine and romidepsin are highly effective in patients with PTCL: a multicenter phase 2 study. *Blood*. 2021;137(16):2161-2170.
10. O'Connor OA, Falchi L, Lue JK, et al. Oral 5-azacytidine and romidepsin exhibit marked activity in patients with PTCL: a multicenter phase 1 study. *Blood*. 2019;134(17):1395-1405.
11. Jain S, Jirau-Serrano X, Zullo KM, et al. Preclinical pharmacologic evaluation of pralatrexate and romidepsin confirms potent synergy of the combination in a murine model of human T-cell lymphoma. *Clin Cancer Res*. 2015;21(9):2096-2106.
12. Scotto L, Kinahan C, Douglass E, et al. Targeting the T-cell lymphoma epigenome induces cell death, cancer testes antigens, immune-modulatory signaling pathways. *Mol Cancer Ther*. 2021;20(8):1422-1430.
13. Coiffier B, Pro B, Prince HM, et al. Results from a pivotal, open-label, phase II study of romidepsin in relapsed or refractory peripheral T-cell lymphoma after prior systemic therapy. *J Clin Oncol*. 2012;30(6):631-636.
14. Piekarz RL, Frye R, Prince HM, et al. Phase 2 trial of romidepsin in patients with peripheral T-cell lymphoma. *Blood*. 2011;117(22):5827-5834.
15. Kamaly N, Xiao Z, Valencia PM, Radovic-Moreno AF, Farokhzad OC. Targeted polymeric therapeutic nanoparticles: design, development and clinical translation. *Chem Soc Rev*. 2012;41(7):2971-3010.
16. Ben-Akiva E, Est Witte S, Meyer RA, Rhodes KR, Green JJ. Polymeric micro- and

nanoparticles for immune modulation. *Biomater Sci*. 2018;7(1):14-30.

17. Cheng CJ, Tietjen GT, Saucier-Sawyer JK, Saltzman WM. A holistic approach to targeting disease with polymeric nanoparticles. *Nat Rev Drug Discov*. 2015;14(4):239-247.

18. Ye W, Zhu F, Cai Y, et al. Improved paclitaxel delivery with PEG-b-PLA/zein nanoparticles prepared via flash nanoprecipitation. *Int J Biol Macromol*. 2022;221:486-495.

19. Ibrahim AH, Ibrahim HM, Elbahwy IA, Afouna MI, Tagami T, Ozeki T. Lyophilized tablets of felodipine-loaded polymeric nanocapsules to enhance aqueous solubility: formulation and optimization. *J Drug Deliv Sci Technology*. 2022;70:103172.

20. Ji J, Qin H, Yang Y, Wu J, Wu J. The targeting imaging and treatment capacity of gelsolin-targeted and paclitaxel-loaded PLGA nanoparticles in vitro and in vivo. *Front Bioeng Biotechnol*. 2022;10:933856.

21. Barichello JM, Morishita M, Takayama K, Nagai T. Encapsulation of hydrophilic and lipophilic drugs in PLGA nanoparticles by the nanoprecipitation method. *Drug Dev Ind Pharm*. 1999;25(4):471-476.

22. Fessi H, Puisieux F, Devissaguet JP, Ammoury N, Benita S. Nanocapsule formation by interfacial polymer deposition following solvent displacement. *Int J Pharmaceutics*. 1989;55:1-4.

23. Bhatia SN, Chen X, Dobrovolskaia MA, Lammers T. Cancer nanomedicine. *Nat Rev Cancer*. 2022;22(10):550-556.

24. Tang L, Yang X, Yin Q, et al. Investigating the optimal size of anticancer nanomedicine. *Proc Natl Acad Sci U S A*. 2014;111(43):15344-15349.

25. Fang J, Nakamura H, Maeda H. The EPR effect: unique features of tumor blood vessels for drug delivery, factors involved, and limitations and augmentation of the effect. *Adv Drug Deliv Rev*. 2011;63(3):136-151.

26. Edlund U, Albertsson A-C. *Degradable polymer microspheres for controlled drug delivery. Degradable Aliphatic Polyesters*. 1st ed. Springer Berlin Heidelberg; 2002:67-112.

27. Musumeci T, Ventura CA, Giannone I, et al. PLA/PLGA nanoparticles for sustained release of docetaxel. *Int J Pharm*. 2006;325(1-2):172-179.

28. Danhier F, Ansorena E, Silva JM, Coco R, Le Breton A, Préat V. PLGA-based nanoparticles: an overview of biomedical applications. *J Control Release*. 2012;161(2):505-522.

29. Demento SL, Eisenbarth SC, Foellmer HG, et al. Inflammasome-activating nanoparticles as modular systems for optimizing vaccine efficacy. *Vaccine*. 2009;27(23):3013-3021.

30. Deng WJ, Yang XQ, Liang YJ, et al. FG020326-loaded nanoparticle with PEG and PDLLA improved pharmacodynamics of reversing multidrug resistance in vitro and in vivo. *Acta Pharmacol Sin*. 2007;28(6):913-920.

31. Istodax. Package insert. Bristol Myers Squibb; 2009.

32. Mugheirbi NA, Paluch KJ, Tajber L. Heat induced evaporative antisolvent nanoprecipitation (HIEAN) of itraconazole. *Int J Pharm*. 2014;471(1-2):400-411.

33. Keck CM, Müller RH. Drug nanocrystals of poorly soluble drugs produced by high pressure homogenisation. *Eur J Pharm Biopharm*. 2006;62(1):3-16.